Observation of topological surface states and strong electron/hole imbalance in extreme magnetoresistance compound LaBi

J. Jiang,[1,2,3,4] N. B. M. Schröter,[2] S.-C. Wu,[5] N. Kumar,[5] C. Shekhar,[5] H. Peng,[2] X. Xu,[6] C. Chen,[2] H. F. Yang,[7] C.-C. Hwang,[4] S.-K. Mo,[3] C. Felser,[5] B. H. Yan,[5] Z. K. Liu,[1] L. X. Yang,[6] and Y. L. Chen[1,2,6,*]

[1]*School of Physical Science and Technology, ShanghaiTech University and CAS-Shanghai Science Research Center, Shanghai, China*

[2]*Department of Physics, University of Oxford, Oxford OX1 3PU, United Kingdom*

[3]*Advanced Light Source, Lawrence Berkeley National Laboratory, Berkeley, California 94720, USA*

[4]*Pohang Accelerator Laboratory, POSTECH, Pohang 790-784, Korea*

[5]*Max Planck Institute for Chemical Physics of Solids, D-01187 Dresden, Germany*

[6]*State Key Laboratory of Low Dimensional Quantum Physics, Department of Physics, Tsinghua University, Beijing 100084, China*

[7]*State Key Laboratory of Functional Materials for Informatics, SIMIT, Chinese Academy of Sciences, 865 Changning Road, Shanghai 200050, China*

(Received 13 August 2016; revised manuscript received 15 May 2017; published 6 February 2018)

The recent discovery of the extreme magnetoresistance (XMR) in the nonmagnetic rare-earth monopnictides LaX (X = P, As, Sb, Bi,), a recently proposed new topological semimetal family, has inspired intensive research effort in the exploration of the correlation between the XMR and their electronic structures. In this work, using angle-resolved photoemission spectroscopy to investigate the three-dimensional band structure of LaBi, we unraveled its topologically nontrivial nature with the observation of multiple topological surface Dirac fermions, as supported by our *ab initio* calculations. Furthermore, we observed substantial imbalance between the volume of electron and hole pockets, which rules out the electron-hole compensation as the primary cause of the XMR in LaBi.

DOI: 10.1103/PhysRevMaterials.2.024201

The recent discovery of three-dimensional (3D) topological Dirac and Weyl semimetals [1–6] has inspired great research in the emergent field of topological semimetals (TSMs). Different from topological insulators (TIs) where the topological surface states (TSSs) form Dirac fermions in the bulk gap [7,8], TSMs host bulk states which possess 3D Dirac or Weyl fermions with linear dispersions [9–11]. Moreover, the TSSs in TSMs can survive without a full global bulk gap [12], and even overlaps with the bulk band [13].

Recently, the rare-earth monopnictide LaX (X = P, As, Sb, Bi) [12,14] was proposed to be a new family of TSMs with nontrivial TSSs. While the topology of its bands can be described by a Z_2 invariant as in TIs, a global bulk band gap is absent in LaX. The discovery of extremely large anisotropic magnetoresistance (XMR) up to 10^5% [15,16] in these nonmagnetic compounds further urges an understanding of the correlation between XMR and their electronic structures, which will not only help reveal the mechanism of XMR, but also be instructive for the material search and future device applications.

Currently, the mechanism of XMR in these compounds is still under debate between carrier compensation and topological protection [16–20]. To further complicate the situation, a mechanism of massive divergence between electron and hole mobility favored by moderate carrier compensation has also been proposed in a cousin (topologically trivial) material YSb [19]. Furthermore, existing angle-resolved photoelectron spectroscopy (ARPES) studies on LaSb [20] and YSb [19] suggest that the spin-orbit coupling (SOC) in these compounds is too weak to induce a band inversion, which makes them topologically trivial. Similar ARPES studies on related compounds show initial evidence for surface Dirac fermions; however, the details of these TSSs are still controversial due to the hybridization between the rich metallic bulk bands and the TSSs [12,21–24].

In this work, by conducting high-resolution ARPES experiments, we systematically studied the electronic structure of the heaviest lanthanum monopnictide, LaBi, which has the strongest SOC. We clearly observed TSSs centered at $\bar{\Gamma}$ and $\bar{M}$ in the surface Brillouin zone (BZ), which can be well reproduced by our *ab initio* calculations, thus confirming the nontrivial topology of its electronic structures. Furthermore, by mapping out the Fermi surfaces (FSs) of the electron and hole pockets in the 3D BZ, we found that the volumes of the electron and hole pockets are of substantial difference ($V_e/V_h = 0.3 \pm 0.1$), thereby challenging the perfect electron-hole compensation as the primary mechanism for the XMR in this material.

High-quality LaBi single crystals were synthesized by the Bi flux method [16]. ARPES measurements were performed at beamline I05 of the Diamond Light Source (DLS) and beamline 10.0.1 of the Advanced Light Source (ALS) with an overall energy resolution better than 20 meV and a base pressure better than 1.5×10^{-10} Torr. Density-functional theory as implemented in the Vienna *ab initio* simulation package [25,26] with hybrid functional [27] was adopted for the

*yulin.chen@physics.ox.ac.uk

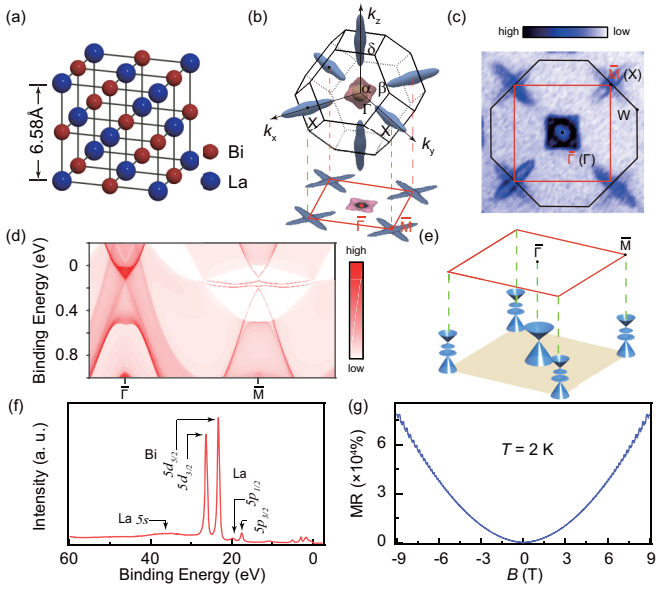

FIG. 1. (a) Crystal structure of LaBi. (b) Bulk FS with its projection on the surface BZ. (c) FS measured with 128-eV photons, the bulk and surface BZ are plotted in black and red, respectively. (d) Our *ab initio* slab calculation projected on the surface. (e) Illustration of the three surface Dirac cones. (f) Core-level spectrum of LaBi. (g) MR measured at 2 K up to 9 T, showing the nonsaturate XMR behavior.

bulk electronic structure calculations. SOC was included in all calculations. The parameters from maximally localized Wannier functions [28–30] were used to interpolate the bulk FSs and the band structures. For the calculation of the surface states (SSs), half-infinite slabs were used with the Green's function method based on the parameters from Wannier functions.

LaBi crystallizes in a simple face-centered rock-salt structure (space group $F_{m\bar{3}m}$) with a lattice constant $a = b = c = 6.58$ Å, illustrated in Fig. 1(a). The BZ of LaBi together with the bulk FS from our *ab initio* calculations, as well as their projection on the (001) surface BZ, are shown in Fig. 1(b). Theoretically, there are two hole pockets at Γ and one electron pocket at X in the bulk BZ. The projection of these pockets on the surface BZ results in a superposition of multiple pockets, which leads to circular and intersecting elliptical pockets at $\bar{\Gamma}$ and a crosslike feature at $\bar{M}$. Due to the momentum broadening along k_z, our measured FS also shows the projections from multiple FS pockets [Fig. 1(c)], consistent with the projection in Fig. 1(b). In addition to the metallic bulk bands, our *ab initio* calculation shows multiple SSs [Figs. 1(d) and 1(e)] at $\bar{\Gamma}$ and $\bar{M}$, which reflects its topologically nontrivial nature. Figure 1(f) shows the core-level spectrum of our sample, which displays the characteristic La $5p/5s$ and Bi $5d$ peaks. We observed an XMR as large as 75 000%, which presents a B-square behavior without saturation at 2 K under 9 T in our sample in Fig. 1(g), consistent with previous reports [16,18].

Figure 2 shows the band structure in the XΓX plane [indicated in blue in Fig. 2(a)]. (For details about the k_z correspondence see the Supplemental Material, SM [31]). The electronic structure is presented in the 3D volume plot in Fig. 2(b), which shows the band dispersions along high-symmetry directions. Figures 2(c) and 2(d) compare our measured equal energy contours with our calculations at different binding energies, which show a good agreement regarding the detailed shape and size of the pockets around Γ. However, while our calculated electron pockets agree qualitatively with the experiment, they are slightly larger than our measurements. The high-symmetry cuts along the XΓX and XWX directions in our calculation are shown in Fig. 2(e). The two bands forming the holelike pockets at Γ are indicated as α and β, and the band forming the electronlike pocket around X is indicated as δ. We emphasize that our calculation shows a projected bulk band gap at X between δ and β ($0.2\ \text{eV} < E_B < 0.5\ \text{eV}$), which results from the band inversion between these two bands. The band dispersion along the ΓXΓ direction is shown in Fig. 2(f) together with its second derivative spectra. The measured α, β, and δ bands are consistent with the calculation shown in Fig. 2(e1), and cross the Fermi energy at momenta $k_F^{\alpha} = 0.14 \pm 0.02\ \text{Å}^{-1}$, $k_F^{\beta} = 0.26 \pm 0.02\ \text{Å}^{-1}$, $k_F^{\delta} = 0.57 \pm 0.02\ \text{Å}^{-1}$ (see SM). Remarkably, the band dispersions of β and δ in Fig. 2(f) show an anticrossing along ΓX, which indicates the predicted band inversion in this material [14]. The projected bulk band gap in Fig. 2(e1) is clearly observed and highlighted by a red dashed box in Fig. 2(f2). Furthermore, in our data we clearly detect an in-gap state near X (highlighted with a red arrow), which will be discussed in detail later. We also detect a Dirac cone at Γ as highlighted in Fig. 2(f2), which is also absent in the bulk calculation and is attributed to the SS. Another cut along the XWX direction is shown in Fig. 2(g), which also reveals the above-mentioned SS in the projected band gap at X.

To investigate the 3D electronic structure of LaBi in the bulk BZ, Fig. 3 presents the band structure in the WXW high-symmetry plane [indicated in blue in Fig. 3(a)]. The 3D volume plot in Fig. 3(b) shows the band dispersions along high-symmetry directions. Similar to the results in the XΓX plane, the measured energy contours in Fig. 3(c) are in good agreement with our calculations in Fig. 3(d), although the electron pocket is slightly smaller in the experiment. The band dispersion along the XWX direction and the corresponding second derivative spectrum in Fig. 3(e) are in good agreement with the bulk calculation in Fig. 2(e2). Moreover, the bands show a clear discontinuity at $E_B = 0.5$ eV [indicated by the black arrow in Fig. 3(e1)]. This discontinuity is caused by the band top of β, which is located at the X point near $E_B = 0.5$ eV [Fig. 2(e2)]. Above the β band top, we can again clearly detect the presence of an in-gap state between $E_B = 0.2 \sim 0.5$ eV. The electron pocket δ corresponds to the shorter axis of the elliptical electron pocket centered at X, which crosses the Fermi energy (E_F) at $k_F^{\delta} = 0.05 \pm 0.02\ \text{Å}^{-1}$.

Having gained a comprehensive picture of the bulk band structure of LaBi, we can determine the ratio of the electronlike and holelike carrier densities by fitting the cross sections of the three bulk FSs (see SM [31]). We inferred their 3D volumes as $V_{\alpha} = 0.012\ \text{Å}^{-3}$, $V_{\beta} = 0.030\ \text{Å}^{-3}$, and $V_{\delta} = 0.004\ \text{Å}^{-3}$, resulting in an electron/hole concentration ratio of about 0.3 ± 0.1 (see SM [31]). Our result gives the hole and electron carrier density as $n_h = 3.4 \times 10^{20}\ \text{cm}^{-3}$ and $n_e = 0.97 \times 10^{20}\ \text{cm}^{-3}$, respectively. Mass spectrometry analysis of another LaBi sample showed ~1% lanthanum deficiency, which according

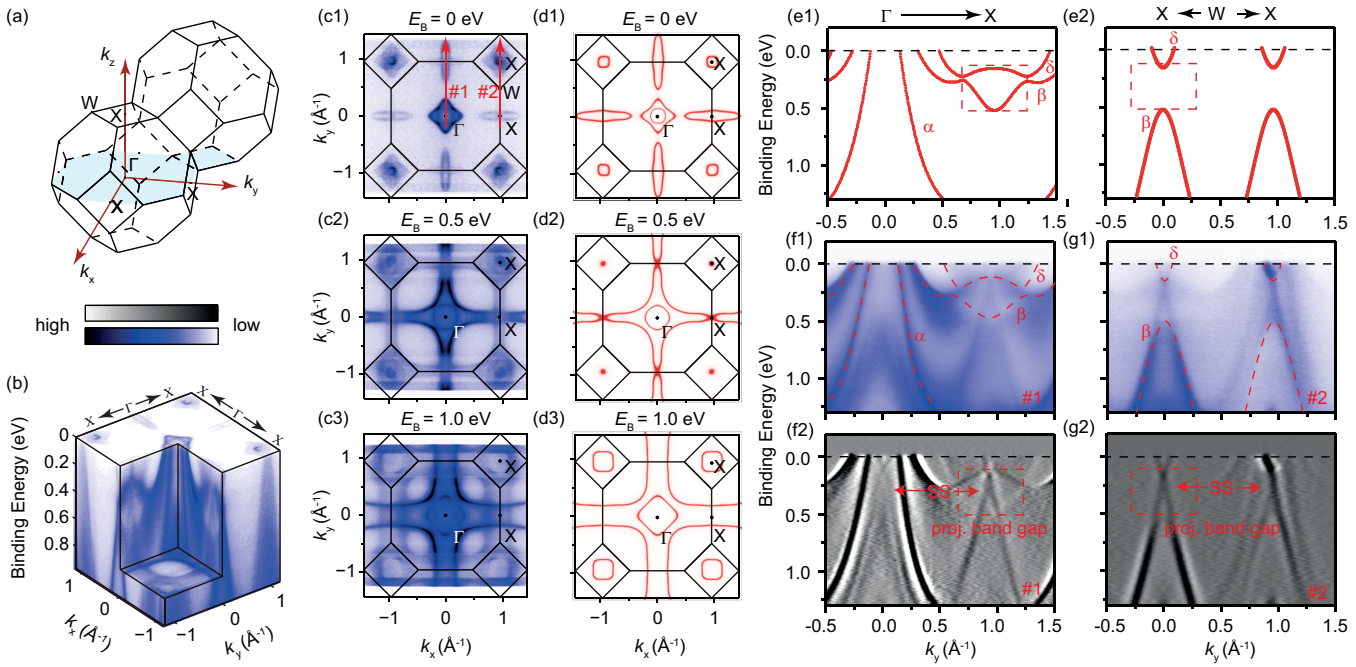

FIG. 2. (a) Illustration of the XΓX plane in the bulk BZ highlighted in blue. (b) 3D volume plot of the bands. (c1–c3) The constant energy contours at $E_B = 0$ eV, 0.5 eV, and 1.0 eV, respectively. (d1–d3) The corresponding *ab initio* calculation results in (c). (e1) Calculated bulk band dispersions along XΓX and (e2) XWX. (f1) Cut along the XΓX direction indicated as #1 in (c1). (f2) the corresponding second derivative spectrum. (g1) Cut along the XWX direction indicated as #2 in (c1). (g2) The corresponding second derivative spectrum. The red dashed box highlights the projected bulk band gap in which SSs exist.

to our *ab initio* calculations causes a Fermi energy shift of ∼20 meV, which leads to an electron/hole density ratio of 0.8. Assuming approximate linearity, our sample measured with ARPES discussed here ($n_e/n_h \approx 0.3$) should have a lanthanum deficiency of ∼3.5%, while another sample measured with ARPES ($n_e/n_h \approx 0.6$, see supplementary Fig. S8 [31]) should have a lanthanum deficiency of ∼2%. This finding suggests that the lanthanum deficiency between samples can vary in the range of a few percent and cause a large imbalance between electron and hole densities. However, since the XMR appears to be ubiquitous across many samples of LaBi measured by our group and many other groups, our result strongly challenges the perfect carrier compensation as the main mechanism for the observed XMR in LaBi. Notably, although previous quantum oscillation measurements favored the calculated perfect carrier compensation, it observed only two frequencies corresponding to the α and δ pockets [16,18,32]. The observed sizes of the two FSs are different from our results. (The Fermi crossing of the α and δ bands is 0.14 Å^{-1} and 0.05 Å^{-1} in our result, compared with 0.13 Å^{-1} and 0.09 Å^{-1} in the quantum oscillation result.) This difference may be caused by a slight shift of the Fermi level (hole doping due to La deficiency) between the samples used for the two measurements, which may be caused by a variation in the lanthanum vacancy concentration between the samples. The electron carrier concentration deduced from transport measurement is around 5×10^{20} cm^{-3} [16,18,32], higher than our ARPES result of 0.97×10^{20} cm^{-3}. Instead, our ARPES measurements over the entire BZ directly map out the complete 3D FS of LaBi, thus providing more reliable information with regard to the FS pockets. Together with the XMR observed in our sample, we believe that the perfect electron-hole compensation should be excluded as the primary cause of XMR in LaBi.

Next we examine the spatial location of the wave function of the observed in-gap states. By scanning a large range of photon energies (30–90 eV) we are able to reconstruct the momentum perpendicular to the sample surface, commonly referred to as k_z (see SM for details [31]). The dispersion along k_z allows us to distinguish between states that are primarily located at the surface (negligible dispersion along k_z) and states that extend into the bulk (dispersive along k_z). Figure 4(a) shows the equal energy surfaces in the k_y-k_z plane, which allows us to identify one SS at $\bar{\Gamma}$ (SS1) and two SSs at different binding energies at $\bar{M}$ (SS2 and SS3) (details can be found in SM [31]). Figure 4(b) shows the equal energy surfaces of the three SSs at different binding energies. The energy dispersion of these surface states are shown in Figs. 4(c)–4(h). The energy positions of the Dirac points can be seen in Figs. 4(d)–4(h). The Dirac point at $\bar{\Gamma}$ is located at $E_1 = 190$ meV, and energy positions of the Dirac points at $\bar{M}$ are $E_2 = 210$ meV and $E_3 = 350$ meV. In accordance with the nontrivial Z_2 classification of the LaBi bulk bands [14], we find an odd number of SSs at time-reversal invariant momenta in the surface BZ, which is a hallmark of its nontrivial topology [33]. We note that there is a quantitative difference between the exact energy positions of the surface Dirac points in our calculations and experimental results. Such deviations are common, as the *ab initio* calculations we carried out are known to have the following limitations: (1) The exchange-correlation functional is known to show limitations to describe the electron-electron interaction accurately in density-functional theory calculations. (2) The realistic surface boundary conditions may be different from the surface

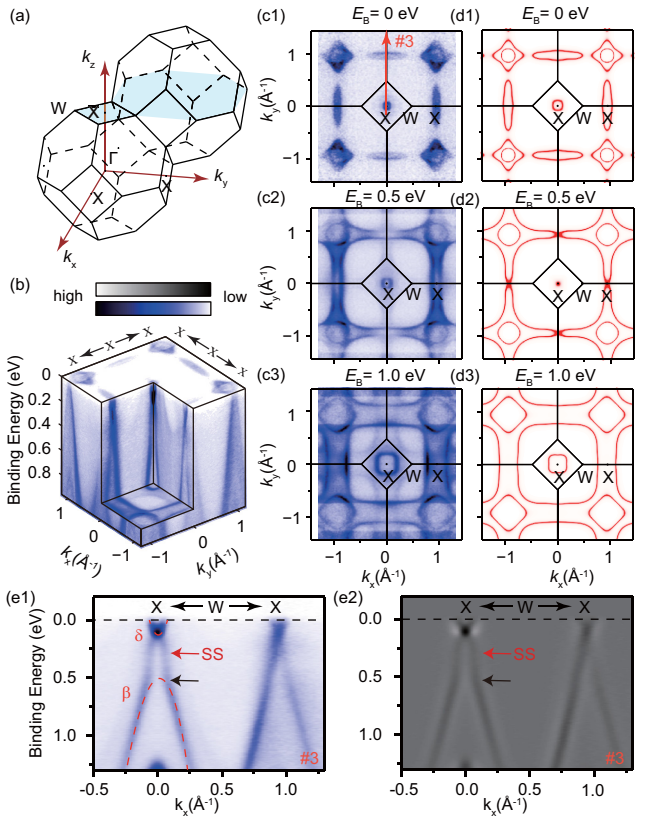

FIG. 3. (a) Illustration of the WXW plane in the bulk BZ highlighted in blue. (b) 3D volume plot of the bands. (c1–c3) The constant energy contours at $E_B = 0$ eV, 0.5 eV, and 1.0 eV, respectively. (d1–d3) The corresponding *ab initio* calculation results in panel (c). (e1) Cut along the XWX direction, indicated as #3 in (c1). (e2) The corresponding second derivative spectrum. The red dashed lines indicate the β and δ bands. The red arrows indicate the SS in the projected band gap, while the black arrow indicates the discontinuity where the surface states merge into the bulk band top of the β band.

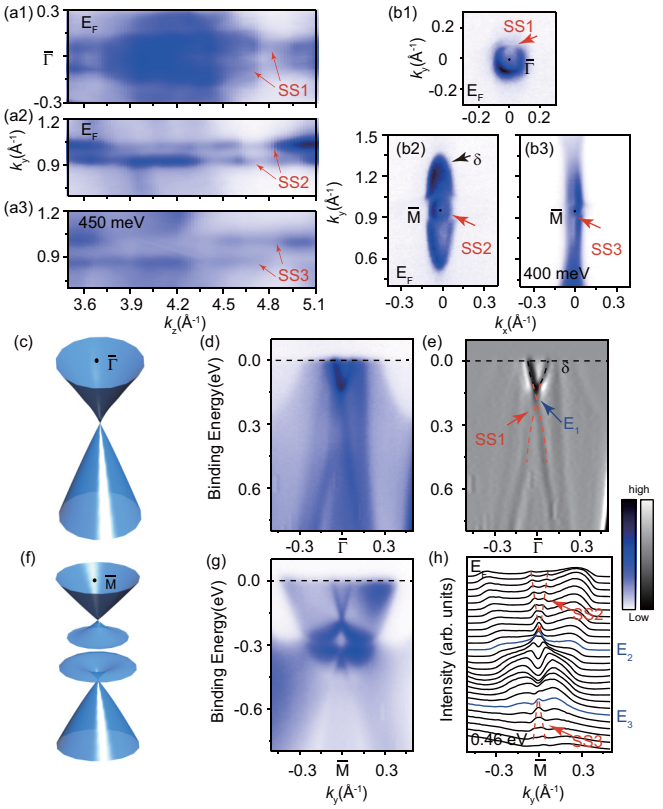

FIG. 4. (a1–a3) Photoemission intensity map along the k_y-k_z plane of SS1, SS2 at E_F and SS3 at $E_B = 450$ meV, respectively. The red arrows indicate the SSs. (b1–b3) Photoemission intensity map along the k_x-k_y plane of SS1, SS2 at E_F and SS3 at $E_B = 400$ meV, respectively. (c) The illustrated band dispersion of the surface Dirac cone at $\bar{\Gamma}$. (d) ARPES result of the band dispersion of the SS at $\bar{\Gamma}$ measured with 54-eV photon. (e) The corresponding second derivative spectra of panel (d). (f) The illustrated band dispersion of the surface Dirac cone at $\bar{M}$. (g) ARPES result of the band dispersion of the SSs at $\bar{M}$. (h) The corresponding momentum distribution curves in panel (g). The three Dirac points' positions are indicated by E_1, E_2, and E_3; SS1, SS2, and SS3 are indicated by the red dashed lines.

termination of a slab model in calculations. This discrepancy can sensitively tune the dispersion of the SSs, including TSSs. However, we do not believe that these qualitative deviations in the energy positions are undermining the central point of our calculation, which shows that the observed odd number of Dirac cones in the projected bulk gap are formed by states located at the sample surface, which is a strong evidence for the nontrivial topology of LaBi.

Finally, we want to discuss the possible mechanism for the emergence of the XMR in LaBi. Besides perfect carrier compensation, two other possibilities have also been proposed. On one hand, a small difference in carrier densities may be counterbalanced by a large difference in carrier mobilities, as has been proposed in YSb ($n_e/n_h = 0.81$) [19]. However, since the difference in carrier densities in LaBi is substantially larger than that in YSb, the required difference in carrier motilities substantially deviates from transport measurements, which can therefore be excluded as a mechanism for the XMR in LaBi (see SM for details [31]). On the other hand, LaBi's nontrivial topology, in combination with a d-p orbital mixing of its bulk electron pockets, has recently been related to the emergence of the XMR [32]. Our polarization-dependent ARPES measurements, which can be found in the SM, indicate the existence of such an orbital mixing [31]. However, to what extent this mechanism is the true origin of the XMR, and whether it can explain its quadratic field dependence, remains to be explored in future studies.

In summary, our finding of TSSs confirms that LaBi stands out as the only lanthanum monopnictide that exhibits topologically nontrivial electronic bulk states. This finding opens the possibility to study topological phase transitions in the LaX family, either by doping LaBi with lighter elements, which leads to weaker SOC, or by applying external pressure, which recently has been shown to lead to the appearance of superconductivity [34] or a metal-insulator transition [35]. Furthermore, the discovery of the nontrivial TSSs and the strong electron/hole volume imbalance in LaBi not only establishes a new family of TSMs, but also leads to the eventual understanding of the underpinned mechanism of the intriguing XMR effect recently found in different nonmagnetic materials families [16,18], as our finding rules out the perfect carrier

compensation scenario as the main origin of the XMR in LaBi, thus putting strong constraints on future theoretical investigations.

We acknowledge the support of a EPSRC Platform Grant (Grant No. EP/M020517/1) and Hefei Science Center CAS (2015HSC-UE013). C.F. acknowledges the support of an ERC Advanced grant (Grant No. 291472). J.J. and C.-C.H. acknowledge the support of the NRF, Korea (Grants No. 2011-0030787 and No. 2017R1A2B2003928). N.B.M.S. acknowledges support from Studienstiftung des Deutschen Volkes. C.C. and H.P. acknowledge the support of a China Scholarship Council–University of Oxford Scholarship. H.F.Y. acknowledges financial support from the Bureau of Frontier Sciences and Education, Chinese Academy of Sciences.

J.J. and N.B.M.S. contributed equally to this work.

[1] Z. K. Liu, B. Zhou, Y. Zhang, Z. J. Wang, H. M. Weng, D. Prabhakaran, S.-K. Mo, Z. X. Shen, Z. Fang, X. Dai, Z. Hussian, and Y. L. Chen, Science **343**, 864 (2015).

[2] Z. K. Liu, J. Jiang, B. Zhou, Z. J. Wang, Y. Zhang, H. M. Weng, D. Prabhakaran, S-K. Mo, H. Peng, P. Dudin, T. Kim, M. Hoesch, Z. Fang, X. Dai, Z. X. Shen, D. L. Feng, Z. Hussain, and Y. L. Chen, Nat. Mater. **13**, 677 (2014).

[3] J. Jiang, Z. K. Liu, Y. Sun, H. F. Yang, C. R. Rajamathi, Y. P. Qi, L. X. Yang, C. Chen, H. Peng, C-C. Hwang, S. Z. Sun, S.-K. Mo, I. Vobornik, J. Fujii, S. S. P. Parkin, C. Felser, B. H. Yan, and Y. L. Chen, Nat. Commun. **8**, 13973 (2017).

[4] Y. Wu, D. X. Mou, N. H. Jo, K. W. Sun, L. N. Huang, S. L. Bud'ko, P. C. Canfield, and A. Kaminski, Phys. Rev. B **94**, 121113 (2016).

[5] L. X. Yang, Z. K. Liu, Y. Sun, H. Peng, H. F. Yang, T. Zhang, B. Zhou, Y. Zhang, Y. F. Guo, M. Rahn, D. Prabhakaran, Z. Hussain, S.-K. Mo, C. Felser, B. H. Yan, and Y. L. Chen, Nat. Phys. **11**, 728 (2015).

[6] Z. K. Liu, L. X. Yang, Y. Sun, T. Zhang, H. Peng, H. F. Yang, C. Chen, Y. Zhang, Y. F. Guo, D. Prabhakaran, M. Schmidt, Z. Hussain, S.-K. Mo, C. Felser, B. H. Yan, and Y. L. Chen, Nat. Mater. **15**, 27 (2016).

[7] Y. L. Chen, J. G. Analytis, J.-H. Chu, Z. K. Liu, S.-K. Mo, X. L. Qi, H. J. Zhang, D. H. Lu, X. Dai, Z. Fang, S. C. Zhang, I. R. Fisher, Z. Hussain, and Z.-X. Shen, Science **325**, 178 (2009).

[8] Y. L. Chen, Front. Phys. **7**, 175 (2012).

[9] X. Wan, A. M. Turner, A. Vishwanath, and S. Y. Savrasov, Phys. Rev. B **83**, 205101 (2011).

[10] Y. Sun, S.-C. Wu, M. N. Ali, C. Felser, and B. Yan, Phys. Rev. B **92**, 161107(R) (2015).

[11] Z. Wang, H. Weng, Q. Wu, X. Dai, and Z. Fang, Phys. Rev. B **88**, 125427 (2013).

[12] J. Nayak, S.-C. Wu, N. Kumar, C. Shekhar, S. Singh, J. Fink, E. E. D. Reinks, G. H. Fecher, S. S. P. Parkin, B. H. Yan, and C. Felser, Nat. Commun. **8**, 13942 (2017).

[13] Z. K. Liu, L. X. Yang, S.-C. Wu, C. Shekhar, J. Jiang, H. F. Yang, Y. Zhang, S.-K. Mo, Z. Hussain, B. H. Yan, C. Felser, and Y. L. Chen, Nat. Commun. **7**, 12924 (2016).

[14] M. Zeng, C. Fang, G. Q. Chang, Y.-A. Chen, T. Hsieh, A. Bansil, H. Lin, and L. Fu, arXiv:1504.03492.

[15] F. F. Tafti, Q. D. Gibson, S. K. Kushwaha, N. Haldolaarachchige, and R. J. Cava, Nat. Phys. **12**, 272 (2016).

[16] N. Kumar, C. Shekhar, S.-C. Wu, I. Leermakers, O. Young, U. Zeitler, B. Yan, and C. Felser, Phys. Rev. B **93**, 241106 (2016).

[17] P.-J. Guo, H.-C. Yang, B.-J. Zhang, K. Liu, and Z.-Y. Lu, Phys. Rev. B **93**, 235142 (2016).

[18] S. Sun, Q. Wang, P.-J. Guo, K. Liu, and H. Lei, New J. Phys. **18**, 082002 (2016).

[19] J. F. He, C. F. Zhang, N. J. Ghimire, T. Liang, C. J. Jia, J. Jiang, S. J. Tang, S. D. Chen, Y. He, S.-K. Mo, C.-C. Hwang, M. Hashimoto, D. H. Lu, B. Moritz, T. P. Devereaux, Y. L. Chen, J. F. Mitchell, and Z. X. Shen, Phys. Rev. Lett. **117**, 267201 (2016).

[20] L.-K. Zeng, R. Lou, D.-S. Wu, Q. N. Xu, P.-J. Guo, L.-Y. Kong, Y.-G. Zhong, J.-Z. Ma, B.-B. Fu, P. Richard, P. Wang, G. T. Liu, L. Lu, Y.-B. Huang, C. Fang, S.-S. Sun, Q. Wang, L. Wang, Y.-G. Shi, H. M. Weng, H.-C. Lei, K. Liu, S.-C. Wang, T. Qian, J.-L. Luo, and H. Ding, Phys. Rev. Lett. **117**, 127204 (2016).

[21] X. H. Niu, D. F. Xu, Y. H. Bai, Q. Song, X. P. Shen, B. P. Xie, Z. Sun, Y. B. Huang, D. C. Peets, and D. L. Feng, Phys. Rev. B **94**, 165163 (2016).

[22] N. Alidoust, A. Alexandradinata, S. Y. Xu, I. Belopolski, S. K. Kushwaha, M. G. Zeng, M. Neupane, G. Bian, C. Liu, D. S. Sanchez, P. P. Shibayev, H. Zheng, L. Fu, A. Bansil, H. Lin, R. J. Cava, and M. Z. Hasan, arXiv:1604.08571.

[23] M. Neupane, M. M. Hosen, I. Belopolski, N. Wakeham, K. Dimitri, N. Dhakai, J.-X. Zhu, M. Z. Hasan, E. D. Bauer, and F. Ronning, J. Phys.: Condens. Matter **28**, 23LT02 (2016).

[24] Y. Wu, T. Kong, L.-L. Wang, D. D. Johnson, D. Mou, L. Huang, B. Schrunk, S. L. Bud'ko, P. C. Canfield, and A. Kaminski, Phys. Rev. B **94**, 081108(R) (2016).

[25] G. Kresse and J. Hafner, Phys. Rev. B **47**, 558 (1993).

[26] G. Kresse and J. Hafner, Phys. Rev. B **48**, 13115 (1993).

[27] J. Heyd, G. E. Scuseria, and M. Ernzerhof, J. Chem. Phys. **118**, 8207 (2003).

[28] N. Marzari and D. Vanderbilt, Phys. Rev. B **56**, 12847 (1997).

[29] I. Souza, N. Marzari, and D. Vanderbilt, Phys. Rev. B **65**, 035109 (2001).

[30] A. A. Mostofi, J. R. Yates, Y.-S. Lee, I. Souza, D. Vanderbilt, and N. Marzari, Comput. Phys. Commun. **178**, 685 (2008).

[31] See Supplemental Material at http://link.aps.org/supplemental/10.1103/PhysRevMaterials.2.024201 for more details about the ARPES data of the LaBi sample used in the manuscript, ARPES data of another sample, and the fitting results of different carrier mobilities in LaBi.

[32] F. F. Tafti, Q. Gibson, S. Kushwaha, J. W. Krizan, N. Haldolaarachchige, and R. J. Cava, Proc. Natl. Acad. Sci. USA **113**, E3475 (2016).

[33] M. Z. Hasan and C. L. Kane, Rev. Mod. Phys. **82**, 3045 (2010).

[34] F. F. Tafti, M. S. Torikachvili, R. L. Stillwell, B. Baer, E. Stavrou, S. T. Weir, Y. K. Vohra, H.-Y. Yang, E. F. McDonnell, S. K. Kushwaha, Q. D. Gibson, R. J. Cava, and J. R. Jeffries, Phys. Rev. B **95**, 014507 (2017).

[35] N. N. Stepnaov, N. V. Morozova, A. E. Kar'kin, I. V. Korobeinikov, A. V. Golubkov, and V. V. Kaminskii, Phys. Solid State **57**, 1639 (2015).